JOURNAL OF Materials CHEMISTRY

B-site cation arrangement and crystal structure of layered perovskite compounds $CsLn_2Ti_2NbO_{10}$ (Ln = La, Pr, Nd, Sm) and $CsCaLaTiNb_2O_{10}$

Young-Sik Hong,*[a] Si-Joong Kim,[b] Seung-Joo Kim[c] and Jin-Ho Choy[c]

[a]*Research Division of Chemistry and Molecular Engineering, Department of Chemistry, Korea University, Sungbuk-Ku, Seoul 136-701, Korea; E-mail: youngsikh@yahoo.com*
[b]*Korea Basic Science Institute, Sungbuk-Ku, Seoul 136-701, Korea*
[c]*Department of Chemistry, Center for Molecular Catalysis, Seoul National University, 151-741 Seoul, Korea*

Received 25th October 1999, Accepted 2nd February 2000

B-site cation arrangement and crystal structure in the layered perovskite compounds $CsLa_2Ti_2NbO_{10}$ (Ln = La, Pr, Nd, Sm) and $CsCaLaTiNb_2O_{10}$ have been investigated by the Rietveld analysis of the powder X-ray diffraction patterns, lattice energy calculations, and intercalation reactions. In $CsLa_2Ti_2NbO_{10}$, equal numbers of Ti^{4+} and Nb^{5+} cations were statistically distributed in the outer octahedra, and only Ti^{4+} cations occupied the middle octahedra. These oxides represent the first example of layered perovskites, in that the B-site cations are distributed in the ordering sequence of Cs–$(Ti_{0.5}Nb_{0.5})O_6$–TiO_6–$(Ti_{0.5}Nb_{0.5})O_6$–Cs in the tripled octahedra. On the other hand, in $CsCaLaTiNb_2O_{10}$, there is a rather complicated fashioning of Cs–$(Ti_{0.15}Nb_{0.85})O_6$–$(Ti_{0.70}Nb_{0.30})O_6$–$(Ti_{0.15}Nb_{0.85})O_6$–Cs, not the ordering sequence of Cs–NbO_6–TiO_6–NbO_6–Cs. It can be demonstrated that the B-site cation arrangement is partly determined by the electrostatic stabilization of the CsO rock salt interlayer, which can be confirmed from the lattice energy calculation. Since half of the NbO_6 in $CsLa_2Ti_2NbO_{10}$ is positioned with half of the TiO_6 in the outer octahedra, its protonated phase, $H_{0.95}Cs_{0.05}La_2Ti_2NbO_{10}\cdot 1.3H_2O$, can be easily reacted with n-alkylamines.

Introduction

Since the discovery of perovskite-structured layered compounds, such as Aurivillius and Ruddlesden–Popper phases, many compounds with perovskite-based $A_{n-1}B_nO_{3n+1}$ layers have been described.[1,2] In 1981, Dion *et al.* synthesized a new family of the layered oxides, $MCa_2Nb_3O_{10}$ (M = K, Rb, Cs, Tl) with the general formula $MA_{n-1}B_nO_{3n+1}$.[3] These compounds also consist of $A_{n-1}B_nO_{3n+1}$ layers, which are separated by large M cations along one of the perovskite cubic directions. Subsequently, a series of compounds, $M[Ca_2Na_{n-3}Nb_nO_{3n+1}]$ (M = K, Rb, Cs and n = 3–7),[4] have been synthesized and named after the Dion–Jacobson series. Other related oxides, such as $MLaNb_2O_7$ (M = Li, Na, K, Rb, Cs, NH_4), $MBiNb_2O_7$ and $MPb_2Nb_3O_{10}$ (M = Rb, Cs), $KCa_2(Ca,Sr)_{n-3}Nb_3Ti_{n-3}O_{3n+1}$ (n = 4, 5), $K_{1-x}La_xCa_{2-x}Nb_3O_{10}$, $MCa_2Nb_{3-x}Fe_xO_{10-x}$ (M = Rb, Cs), and $KSr_2Nb_3O_{10}$, have also been characterized.[5–10]

It is also well known that such compounds have a cationic exchange capacity in molten salts or in acidic solutions. Their protonated phases, which have attracted much attention in the area of intercalation chemistry, are known to exhibit acid catalytic and photo-catalytic activities for the evolution of H_2 gas from an aqueous solution of methanol.[11,12] Therefore, it is very important to understand the factors for controlling the acidity of solid oxides since the rational design of acid catalysts for specific purposes is possible. One conclusive factor is the layer charge density in $[A_{n-1}B_nO_{3n+1}]$ layer. For example, the compounds of the Dion–Jacobson series, $M[A_{n-1}B_nO_{3n+1}]$, are more acidic than those of the Ruddlesden–Popper series, $M_2[A_{n-1}B_nO_{3n+1}]$, because of their lower layer charge density.[13,14] The other is the character of the metal–oxygen bonding, as shown by the acidity order of $HNb_3O_8\cdot H_2O > HTiNbO_5 > H_2Ti_4O_9$.[15] Such a difference apparently comes from the bond character of the octahedra bound to protons, that is, the protons attached to NbO_6 are assumed to be more acidic than those attached to TiO_6.

Based on the bond character of the octahedra, Gopalakrishnan *et al.* have argued that the acidity in $HCaLaTiNb_2O_{10}$ with the ordering sequence H–NbO_6–TiO_6–NbO_6–H is higher than in $HLa_2Ti_2NbO_{10}$ with H–TiO_6–NbO_6–TiO_6–H.[15] We have also proposed a model in which the B-site cations are statistically distributed in two crystallographic sites.[16] Until now, however, no reports have addressed the B-site cation arrangements, though many compounds with mixed cations in the B-site, such as $MCa_2Na_{n-3}Nb_nO_{3n+1}$, $MCa_2Nb_{3-x}Fe_xO_{10-x}$, $MCa_{2-x}La_xTi_xNb_{3-x}O_{10}$, $M_{2-x}La_2Ti_{3-x}Nb_xO_{10}$ and $RbLaSrNb_2CuO_9$, have been synthesized.[4,9,15,17]

In this work, we have been able to demonstrate, for the first time, that equal numbers of Ti^{4+} and Nb^{5+} cations are statistically distributed in the outer octahedra with only Ti^{4+} occupying the middle octahedra in $CsLn_2Ti_2NbO_{10}$ (Ln = La, Pr, Nd, Sm). In fact, we have been successful in realizing the intercalation reaction in its protonated compound with n-alkylamines.

Experimental

The compounds $CsLn_2Ti_2NbO_{10}$ (Ln = La, Pr, Nd, Sm) and $CsCaLaTiNb_2O_{10}$ were prepared by conventional solid-state reaction. The starting materials were Cs_2CO_3, $CaCO_3$, La_2O_3, Pr_6O_{11}, Nd_2O_3, Sm_2O_3, TiO_2, and Nb_2O_5. An excess amount of Cs_2CO_3 (25 mol%) was added to compensate for the loss due to the volatilization of the caesium component. The reactants were ball-milled in ethanol for 12 h and then calcined between 1050 °C and 1150 °C for 24 h in alumina crucibles. The protonated phase was prepared by ion exchange with aqueous 4 M HCl solution at 60 °C for 4 days. The product was refluxed

DOI: 10.1039/a908454a

with 10% n-alkylamine in water or in heptane for 3 days at 60–90 °C.

Powder X-ray diffraction data were recorded at room temperature on a Philips X'pert MPD using Bragg–Brentano geometry with Cu K_α radiation. Step scans were performed over the angular range $10 < 2\theta/^\circ < 110$ with a step size of 0.02° and a counting time of 10 s. The compounds were refined by the Rietveld method using the FULLPROF program.[18] The peak shape was described by a pseudo-Voigt function. The background level was defined by a polynomial function. For each diffraction pattern, the scale factor, the counter zero point, the peak asymmetry and the unit-cell dimensions were refined in addition to the atomic parameters. Elemental analysis using energy-dispersive X-ray emission gave a stoichiometric composition within experimental errors. The organic contents of the intercalates were determined by thermogravimetry (TG; Stanton Redcroft TGA-1000).

Results and discussion

$CsLa_2Ti_2NbO_{10}$

All the peaks of the X-ray diffraction patterns were indexed on a tetragonal cell with $a = 3.850$ Å and $c = 15.393$ Å. There were no reflection conditions for this indexing, leading to the space group *P4/mmm*. As mentioned above, there are two controversial arguments for the B-site cation arrangement in $CsLa_2Ti_2NbO_{10}$. In fact, Ti^{4+} and Nb^{5+} cations can be crystallographically distributed over two independent sites; 1a (0,0,0) and 2g (0,0, ~0.28). This indicates that three models for the B-site cation arrangement can be proposed, as shown in Fig. 1, depending on the distribution of the two cations. Fig. 2 shows the observed and calculated powder X-ray diffraction profiles of the selected 2θ ranges of $CsLa_2Ti_2NbO_{10}$. In the first stage, the refinement was carried out using the initial atomic position of $CsCa_2Ta_3O_{10}$.[19] In model 1, Ti^{4+} and Nb^{5+} cations occupy the 1a and 2g sites, respectively, and the refinement gives the agreement factors of $R_p = 20.0\%$, $R_{wp} = 28.5\%$, and $R_I = 15.1\%$. Model 2 was adopted to improve the refinement, but all the agreement factors, $R_p = 12.7\%$, $R_{wp} = 15.1\%$, and $R_I = 6.52\%$, were still high. The refinement was carried out by introducing model 3, where TiO_6 octahedra are flanked by the

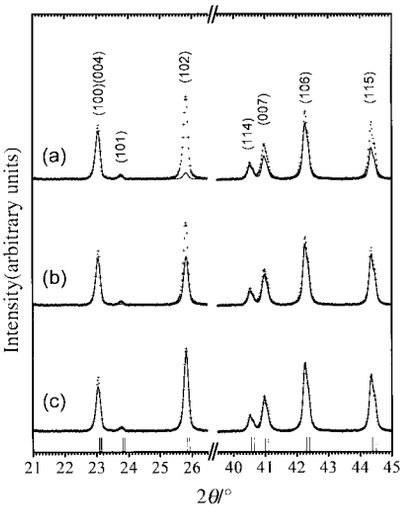

Fig. 2 Selected observed and calculated powder X-ray diffraction profiles of $CsLa_2Ti_2NbO_{10}$, according to (a) model 1, (b) model 2 and (c) model 3.

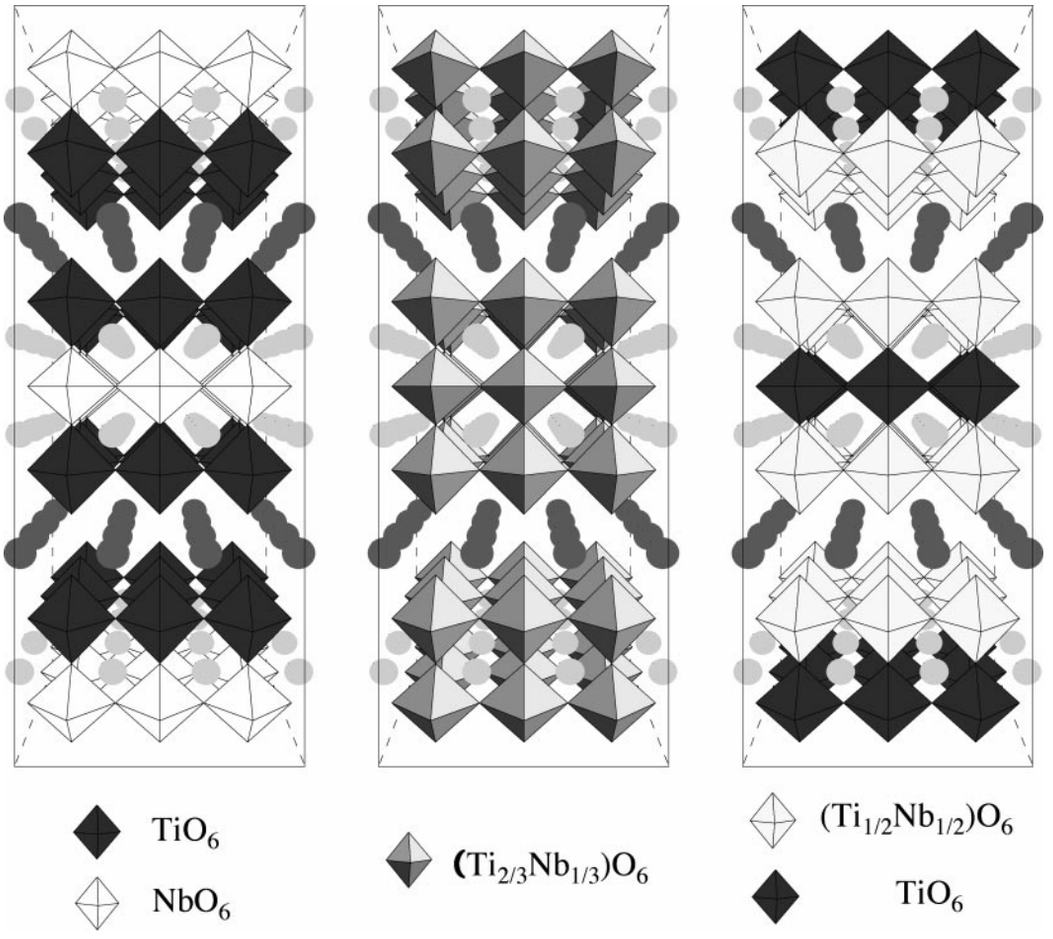

Fig. 1 Three models for B-site cation arrangement in $CsLa_2Ti_2NbO_{10}$. (a) Model 1, Cs–TiO_6–NbO_6–TiO_6–Cs; (b) model 2, Cs–$(Ti_{0.67}Nb_{0.33})O_6$–$(Ti_{0.67}Nb_{0.33})O_6$–$(Ti_{0.67}Nb_{0.33})O_6$–Cs; and (c) model 3, Cs–$(Ti_{0.5}Nb_{0.5})O_6$–TiO_6–$(Ti_{0.5}Nb_{0.5})O_6$–Cs.

outer $(Ti_{0.5}Nb_{0.5})O_6$ octahedra, Fig. 1(c). The agreement factors improved significantly: $R_p = 9.44\%$, $R_{wp} = 11.8\%$, and $R_I = 3.15\%$. Finally, the site occupancies of Ti^{4+} and Nb^{5+} cations were refined, but no significant deviation from the composition of model 3 was found. It can be concluded that the distribution of B-site cations in octahedra has the new-type ordering sequence of Cs–$(Ti_{0.5}Nb_{0.5})O_6$–TiO_6–$(Ti_{0.5}Nb_{0.5})O_6$–Cs.

Whether the B′ and B″ site cations are ordered or disordered in the perovskites, $A(B'_{1/2}B''_{1/2})O_3$, it is necessary to know the magnitude of the difference in the ionic radii and in the charges between the B′ and B″ cations. If the differences are large, the ordering arrangement would be more favorable due to a gain of lattice energy. In this regard, it is noteworthy that, for the first time, the new-type ordering sequence in $CsLa_2Ti_2NbO_{10}$ was found even though the differences in size and charge are not significant at all. At this stage, it is necessary to explain why such an ordering appeared in the layered perovskite. Let us imagine the compound $CsLa_2Ti_2NbO_{10}$ as the composite of a CsO rock salt layer and a $La_2Ti_2NbO_9$ perovskite layer. Then, it can be simply depicted as a chain of $[CsO]^{-1}$–$[La_{0.5}(Ti_{1-x}Nb_x)O_3]^{x-0.5}$–$[La(Ti_{2x}Nb_{1-2x})O_3]^{-2x+2}$–$[La_{0.5}(Ti_{1-x}Nb_x)O_3]^{x-0.5}$–$[CsO]^{-1}$, depending on the distribution of B-site cations. Assuming that $x = 0.5$, it gives the charge distribution of $[CsO]^{-1}$–$[La_{0.5}(Ti_{0.5}Nb_{0.5})O_3]^0$–$[LaTiO_3]^{+1}$–$[La_{0.5}(Ti_{0.5}Nb_{0.5})O_3]^0$–$[CsO]^{-1}$ with the ideal charge separation. It can be concluded that the insertion of a CsO layer with negative charge into a 3-dimensional perovskite structure contributes to the new-type ordering of Ti^{4+} and Nb^{5+} cations along the *z*-axis by electrostatic stabilization. Recently, Crosnier-Lopez *et al*. reported on B-site cation arrangement for $Li_2La_{2.25}(Nb_{1.25}Ti_{2.75})O_{13}$ ($n = 4$), where Nb^{5+} and Ti^{4+} cations are statistically occupied in octahedral sites, as generally reported in perovskite lattices.[20] On the other hand, the compound $Li_2La_{1.78}(Nb_{0.66}Ti_{2.34})O_{10}$ ($n = 3$) has a sequence of $[Li_2O]^0$–$[La_{0.445}(Ti_{0.69}Nb_{0.31})O_3]^{-0.355}$–$[La_{0.89}(Ti_{0.96}Nb_{0.04})O_3]^{+0.71}$–$[La_{0.445}(Ti_{0.69}Nb_{0.31})O_3]^{-0.355}$–$[Li_2O]^0$, where most of the Nb^{5+} cations occupy the outer octahedra.[21] This will be explained in a subsequent paper in relation to the Aurivillius phase.

Fig. 3 shows the observed, calculated and difference X-ray diffraction profiles for $CsLa_2Ti_2NbO_{10}$. The refined atomic positions and isotropic thermal parameters are listed in Table 1. The Rietveld refinement for the B-site cation arrangement gave satisfactory results, but certain features remained anomalous. In particular, the four equatorial oxygens, O(1), in the middle octahedra showed large thermal parameters. Such phenomena are generally observed in layered perovskites with a triple layer.[22–24] To gain an insight on this

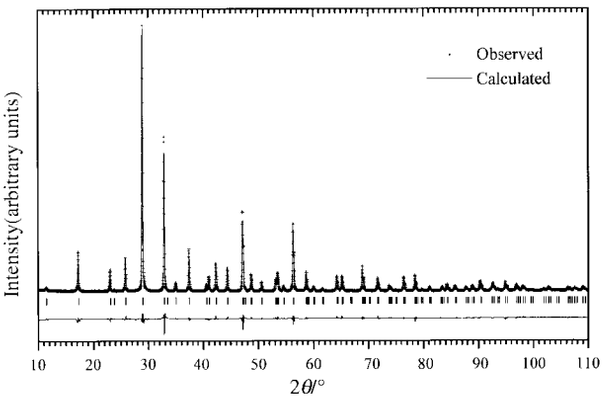

Fig. 3 Observed, calculated and difference powder X-ray diffraction profiles of $CsLa_2Ti_2NbO_{10}$. The Bragg positions are marked.

problem, the bond valence sum calculation was made using the bond distances obtained from refinement. The most commonly adopted empirical expression for the variation of the length d_{ij} of a bond with valence v_{ij} is $\exp[(R_{ij}-d_{ij})/b]$.[25] Here R_{ij} and b are commonly taken to be the bond valence parameters and a universal constant equal to 0.37 Å, respectively. As expected from the large thermal parameter of O(1), the calculated bond valence of 4.5 for Ti(1) is significantly higher than the theoretical value of 4. An acceptable thermal parameter for O(1) was obtained by allowing relaxation off the ⟨100⟩ mirror plane from the fully occupied 2f site to the half-occupied 4n site. The bond valences of Ti(1) and Ti(2)/Nb(2) decreased from 4.50 to 4.21 and from 4.61 to 4.57, approaching the theoretical values of 4 and 4.5, which provide the driving force for rotation around the *c*-axis.[26]

From the concept of the building block, a distortion of the Ti(2)/Nb(2)–O bond, Table 2, toward the CsO layer is explained by charge separation between the CsO and the perovskite layers. Consequently, the distribution of formal charge in CsO–$La_{0.5}(Ti_{0.5}Nb_{0.5})O_3$–$LaTiO_3$–$La_{0.5}(Ti_{0.5}Nb_{0.5})O_3$–CsO is considered as (-1)–$(\delta^+\cdots\delta^-)$–$(+1)$–$(\delta^-\cdots\delta^+)$–(-1), resulting in two different bond lengths. The Ti(2)/Nb(2) cations are significantly displaced from the center of the octahedra. The short Ti(2)/Nb(2)–O bond with highly covalent character would allow a weak competitive Cs–O bond, which gives ionic conductivities.[27] This concept can be applied to the other layered perovskites. Toda *et al*. have reported that the distortion of Ta–O bonds in $Li_xLaTa_2O_7$ ($x = 1$ or 2) becomes less significant with lithium intercalation.[28] In the same way, the distributions of formal charge are viewed as $[LiO]^{-1}$–$[La_{0.5}TaO_3]^{0.5}$–$[La_{0.5}TaO_3]^{0.5}$–$[LiO]^{-1}$ for LiLa-

Table 1 Crystallographic data of $CsLa_2Ti_2NbO_{10}$ and $CsCaLaNb_2TiO_{10}$

	Atom	Site	*g*	*x*	*y*	*z*	B_{iso}/Å^2
$CsLa_2Ti_2NbO_{10}$	Cs	1d	1	0.5	0.5	0.5	1.61(5)
$a = 3.8495(1)$ Å	La	2h	1	0.5	0.5	0.1410(1)	0.58(3)
$c = 15.3927(2)$ Å	Ti(1)	1a	1	0	0	0	0.60(4)
$R_p = 9.12\%$	Ti(2)/Nb(2)	2g	1	0	0	0.2839(1)	0.60(4)
$R_{wp} = 11.7\%$	O(1)	4n	0.5	0.105(3)	0.5	0	0.7(4)
$R_I = 2.61\%$	O(2)	2g	1	0	0	0.1239(5)	1.3(3)
	O(3)	4i	1	0	0.5	0.2496(4)	0.7(2)
	O(4)	2g	1	0	0	0.3945(6)	−0.1(3)
$CsCaLaTiNb_2O_{10}$	Cs	1d	1	0.5	0.5	0.5	2.13(7)
$a = 3.8690(1)$ Å	Ca/La	2h	1	0.5	0.5	0.1366(1)	0.67(6)
$c = 15.2350(5)$ Å	Ti(2)	2g	0.15(1)	0	0	0.2794(1)	0.24(5)
$R_p = 10.1\%$	Nb(2)	2g	0.85(1)	0	0	0.2794(1)	0.24(5)
$R_{wp} = 12.3\%$	Ti(1)	1a	0.3	0	0	0	0.24(5)
$R_I = 3.85\%$	Nb(1)	1a	0.7	0	0	0	0.24(5)
	O(1)	4n	0.5	0.107(5)	0.5	0	2.9(6)
	O(2)	8s	0.25	0.034(19)	0	0.1231(7)	0.7(6)
	O(3)	8t	0.5	0.026(11)	0.5	0.2518(5)	0.2(3)
	O(4)	8s	0.25	0.034(19)	0	0.3986(8)	2.2(6)

Ta_2O_7 and $[Li_2O]^0$–$[La_{0.5}TaO_3]^0$–$[La_{0.5}TaO_3]^0$–$[Li_2O]^0$ for $Li_2LaTa_2O_7$. That is, the charge separation between the $[Li_xO]$ and perovskite layers decreases with lithium intercalation, and the Ta–O bond is less distorted.

$CsCaLaTiNb_2O_{10}$

Fig. 4 shows the observed and calculated powder X-ray diffraction profiles of the selected 2θ ranges of $CsCaLaTiNb_2O_{10}$. When the same procedures are applied to the compound $CsCaLaNb_2TiO_{10}$, the refinement using model 1 gives the best fit of $R_p = 10.9\%$, $R_{wp} = 13.3\%$, and $R_I = 4.14\%$. At first glance, it seems that the B-site cations are ordered in the manner of Cs–NbO_6–TiO_6–NbO_6–Cs, as proposed by Gopalakrishnan *et al.*[15] However, when we tried to refine the site occupancies there was a significant deviation from model 1. According to the results of the refinement on site occupancies, the distribution in $CsCaLaTiNb_2O_{10}$ shows the outer and middle octahedra occupied by the (0.15Ti + 0.85Nb) and (0.70Ti + 0.30Nb) mixed cations, respectively. The refined atomic positions and isotropic thermal parameters are listed in Table 1 and the bond lengths are listed in Table 2. For $CsCaLaTiNb_2O_{10}$, the rotation of the octahedra is simultaneously observed with a minor tilting of the outer octahedra, suggested by the displacements in O(2) and O(4). This type of distortion is typically observed when the A′ cation is too small for the cubic BO_3 corner-sharing octahedral network. In such cases it is the lowest energy distortion mode, because the A–O distances can be softened while the first coordination sphere around the B cation remains unchanged.[29] However, no superstructure reflections, which would be indicative of long-range ordering of these rotations or tilts, were apparent in the X-ray powder diffraction profile. When the $CsCaLaTiNb_2O_{10}$ was annealed to improve the ordering of the B-site cations, it decomposed to a layered perovskite and a pyrochlore compound due to the loss of the caesium component.

One may question why the distribution of B-site cations in $CsCaLaNb_2TiO_{10}$ appears in the mixed distributions of Cs–$Ca_{0.25}La_{0.25}(Ti_{0.15}Nb_{0.85})O_3$–$Ca_{0.5}La_{0.5}(Ti_{0.7}Nb_{0.3})O_3$–$Ca_{0.25}La_{0.25}(Ti_{0.15}Nb_{0.85})O_3$–Cs while that of $CsLa_2Ti_2NbO_{10}$ shows the sequence of Cs–$La_{0.5}(Ti_{0.5}Nb_{0.5})O_3$–$LaTiO_3$–$La_{0.5}(Ti_{0.5}Nb_{0.5})O_3$–Cs. To confirm the distribution of B-site cations, the lattice energy was calculated using the program MADEL (Mackintoshi version) attached in FAT-RIETAN. Fig. 5 shows the calculated lattice energy as a function of the percentage of Ti^{4+} cations in the middle octahedra. It is particularly interesting, and initially surprising, to note that the distribution of B-site cations arrangement with minimum lattice energy is calculated to Cs–$Ca_{0.25}La_{0.25}(Ti_{0.16}Nb_{0.84})O_3$–$Ca_{0.5}La_{0.5}(Ti_{0.68}Nb_{0.32})O_3$–$Ca_{0.25}La_{0.25}(Ti_{0.16}Nb_{0.84})O_3$–Cs for $CsCaLaTiNb_2O_{10}$, while Cs–$La_{0.5}(Ti_{0.5}Nb_{0.5})O_3$–$LaTiO_3$–$La_{0.5}(Ti_{0.5}Nb_{0.5})O_3$–Cs for $CsLa_2Ti_2NbO_{10}$, which are well fitted to the distributions obtained by Rietveld refinement. This can be explained in part by the electrostatic stabilization due to the insertion of the CsO layer with negative charge into the perovskite layer.

Table 2 Selected bond distances (in Å) of $CsLa_2Ti_2NbO_{10}$ and $CsCaLaTiNb_2O_{10}$

$CsLa_2Ti_2NbO_{10}$		$CsCaLaTiNb_2O_{10}$	
Cs–O(4)	8 × 3.169(5)	Cs–O(4)	4 × 3.063(43)
			4 × 3.227(43)
La–O(1)	2 × 3.185(9)	Ca/La–O(1)	2 × 3.137(14)
La–O(1)	2 × 2.649(9)	Ca/La–O(1)	2 × 2.579(11)
La–O(2)	4 × 2.735(1)	Ca/La–O(2)	2 × 2.653(49)
			2 × 2.837(49)
La–O(3)	4 × 2.549(5)	Ca/La–O(3)	2 × 2.538(6)
			2 × 2.686(32)
Ti(2)/Nb(2)–O(2)	1 × 2.463(8)	Ti(2)/Nb(2)–O(2)	1 × 2.385(11)
Ti(2)/Nb(2)–O(3)	4 × 1.996(2)	Ti(2)/Nb(2)–O(3)	4 × 1.982(40)
Ti(2)/Nb(2)–O(4)	1 × 1.704(9)	Ti(2)/Nb(2)–O(4)	1 × 1.821(13)
Ti(1)–O(1)	4 × 1.967(13)	Ti(1)/Nb(1)–O(1)	4 × 1.978(19)
Ti(1)–O(2)	2 × 1.907(8)	Ti(1)/Nb(1)–O(2)	2 × 1.890(11)

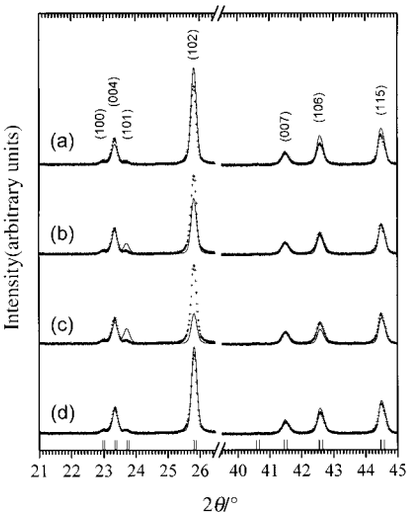

Fig. 4 Selected observed and calculated powder X-ray diffraction profiles of $CsCaLaTiNb_2O_{10}$, according to (a) model 1, (b) model 2, (c) model 3, and (d) occupancy refined.

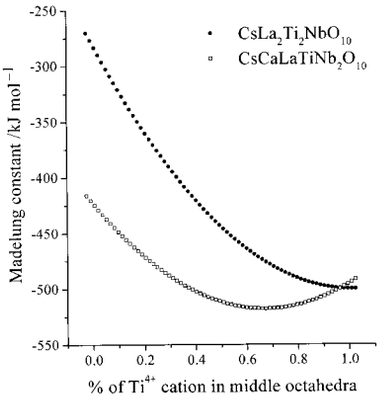

Fig. 5 Lattice energy *versus* percentage of Ti^{4+} cations in the middle octahedra.

$CsLnTi_2NbO_{10}$ (Ln = Pr, Nd, Sm)

The powder X-ray diffraction patterns for $CsLn_2Ti_2NbO_{10}$, where Ln = La, Pr, Nd, Sm, are shown in Fig. 6. The structural refinements for $CsLn_2Ti_2NbO_{10}$ (Ln = Pr, Nd, Sm) using model 3 gave similar results for $CsLa_2Ti_2NbO_{10}$, as listed in Table 3. The thermal parameters of O(2) in $CsLn_2Ti_2NbO_{10}$ (Ln = Pr, Nd, Sm) remained large even though the O(1) site was relaxed to 4n site. It can be demonstrated that the crystal symmetry decreases with the decreasing size of the A-site cations. Although the X-ray characterization described above indicates that the compounds $CsLn_2Ti_2NbO_{10}$ (Ln = Pr, Nd, Sm) are single-phase, a number of unexpected peaks are observed. This suggests that the true symmetry should be lowered from tetragonal to orthorhombic. The structural refinements were carried out using various space groups, such as *Pmma* ($a = \sqrt{2} \times a_p$, $b = c_p$ and $c = \sqrt{2} \times a_p$) and *Imma* ($a = \sqrt{2} \times a_p$, $b = 2 \times c_p$ and $c = \sqrt{2} \times a_p$), where a_p and c_p are the unit-cell parameters in a primitive tetragonal cell. The expansions of the unit cell gave us difficulties with the space group determination due to the systematic absences. This indicates that the extra peaks can be clearly indexed by using the space group *Imma*, as shown in Fig. 7, but this should be further investigated using electron microscopy.

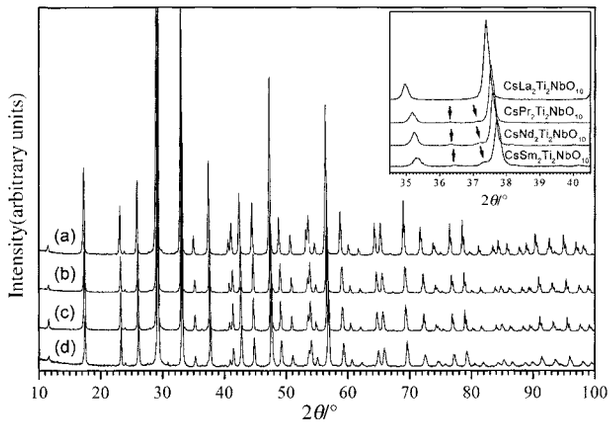

Fig. 6 Powder X-ray diffraction patterns of $CsLn_2Ti_2NbO_{10}$ (Ln = La, Pr, Nd, Sm). The inset shows the limited angular region of 34.5–40.5°.

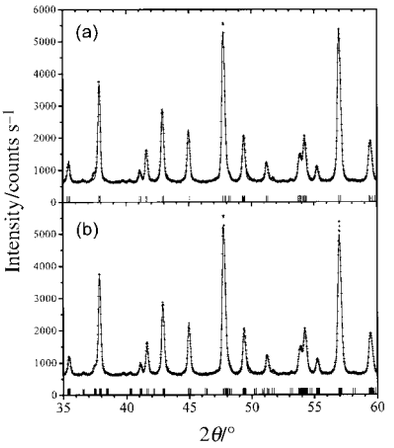

Fig. 7 Observed, calculated and difference powder X-ray diffraction profiles of $CsSm_2Ti_2NbO_{10}$ refined by (a) *P4/mmm* and (b) *Imma*. The Bragg positions are marked.

Protonation and intercalation reactions

Fig. 8 shows the X-ray diffraction patterns of $CsLa_2Ti_2NbO_{10}$, $H_{0.95}Cs_{0.05}La_2Ti_2NbO_{10}\cdot 1.3H_2O$, and intercalates. TG experiments confirmed that the protonated phase is hydrated with $1.3H_2O$. The elemental analysis of the protonated phase revealed that 95% of the caesium ions were replaced, indicating the chemical composition of $H_{0.95}Cs_{0.05}La_2Ti_2NbO_{10}\cdot 1.3H_2O$. n-Alkylamines were intercalated into the protonated phase in water or in heptane. To determine the composition of the intercalates, the amounts of intercalated alkylamines were calculated from the thermogravimetric and elemental analyses, and the proton and caesium atoms were added to neutralize the intercalates (Table 4). The higher order (00*l*) reflections for the intercalates were shifted monotonously to lower 2θ angle with increasing alkyl chain number, indicating the intercalation of alkylamines. The *a* and *c* parameters were calculated from the (200) peak, not shown in Fig. 8, and the least square fits of the (00*l*) peaks, respectively. Since half of the outer octahedra is occupied by the Nb^{5+} cations, the proton in NbO_6–H acts as the solid Brønsted acid, such as $HCa_2Nb_3O_{10}$ and $HTiNbO_5$.[3,29] In fact, many organic amines with $pK_a > 9$ can be intercalated into $H_2Ti_4O_9$ and $HTiNbO_5$. Though Gopalakrishnan *et al.* have rationalized that the compound $HLa_2Ti_2NbO_{10}$ shows little

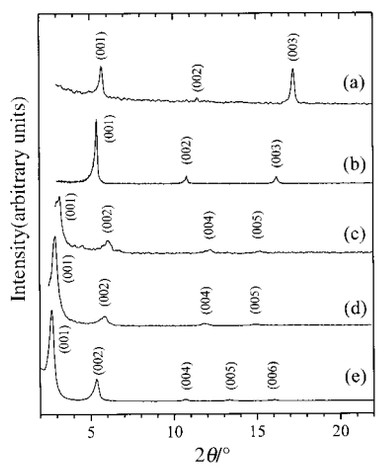

Fig. 8 Powder X-ray diffraction patterns of (a) $CsLa_2Ti_2NbO_{10}$, (b) $H_{0.95}Cs_{0.05}La_2Ti_2NbO_{10}\cdot 1.3H_2O$, (c) n-butylamine-, (d) n-hexylamine- and (e) n-octylamine intercalates.

Table 3 Crystallographic data of $CsLn_2Ti_2NbO_{10}$ (Ln = Pr, Nd, Sm)

	Atom	Site	*x*	*y*	*z*	B_{iso}/Å^2
$CsPr_2Ti_2NbO_{10}$	Cs	1d	0.5	0.5	0.5	1.55(5)
a = 3.8376(1) Å	Pr	2h	0.5	0.5	0.1423(1)	0.66(3)
c = 15.3015(2) Å	Ti(1)	2g	0	0	0.2824(1)	0.37(4)
R_p = 9.55%	Ti(2)/Nb(2)	1a	0	0	0	0.37(4)
R_{wp} = 11.3%	O(1)	4n	0.106(4)	0.5	0	2.1(4)
R_I = 3.06%	O(2)	2g	0	0	0.1240(6)	3.7(4)
	O(3)	4i	0	0.5	0.2472(4)	0.7(2)
	O(4)	2g	0	0	0.3946(6)	1.2(3)
$CsNd_2Ti_2NbO_{10}$	Cs	1d	0.5	0.5	0.5	1.91(6)
a = 3.8319(1) Å	Nd	2h	0.5	0.5	0.1425(1)	1.28(4)
c = 15.2764(3) Å	Ti(1)	2g	0	0	0.2825(1)	0.60(6)
R_p = 12.5%	Ti(2)/Nb(2)	1a	0	0	0	0.60(6)
R_{wp} = 14.3%	O(1)	4n	0.104(5)	0.5	0	3.1(5)
R_I = 5.68%	O(2)	2g	0	0	0.1335(9)	5.8(5)
	O(3)	4i	0	0.5	0.2413(5)	1.7(2)
	O(4)	2g	0	0	0.3985(7)	1.0(3)
$CsSm_2Ti_2NbO_{10}$	Cs	1d	0.5	0.5	0.5	1.7(1)
a = 3.8195(1) Å	Sm	2h	0.5	0.5	0.1426(1)	0.60(6)
c = 15.2371(6) Å	Ti(1)	2g	0	0	0.2829(2)	0.5(1)
R_p = 13.0%	Ti(2)/Nb(2)	1a	0	0	0	0.5(1)
R_{wp} = 15.8%	O(1)	4n	0.124(5)	0.5	0	1.3(1)
R_I = 4.94%	O(2)	2g	0	0	0.1277(10)	6.3(8)
	O(3)	4i	0	0.5	0.2484(7)	1.0(3)
	O(4)	2g	0	0	0.3974(11)	1.5(5)

Table 4 Chemical composition and lattice parameters of protonated phase and intercalates

Compound	*a*/Å	*c*/Å
$H_{0.95}Cs_{0.05}La_2Ti_2NbO_{10}\cdot 1.3H_2O$	3.828	16.462(4)
$[CH_3(CH_2)_2CH_2NH_3]_{0.92}(H,Cs)_{0.08}La_2Ti_2NbO_{10}$	3.825	25.610(6)
$[CH_3(CH_2)_4CH_2NH_3]_{0.90}(H,Cs)_{0.10}La_2Ti_2NbO_{10}$	3.835	29.462(5)
$[CH_3(CH_2)_6CH_2NH_3]_{0.88}(H,Cs)_{0.12}La_2Ti_2NbO_{10}$	3.834	33.300(7)

intercalation behavior due to the lower acidity of TiO_6–H,[15] this should be revised as evidenced by our study. From the basal spacing of intercalates, the tilting angle of the alkyl chain with respect to the inorganic layer surface could be estimated as 49.2°, forming a bilayer in the intercalates.

We have synthesized a series of layered perovskites of $CsLn_2Ti_2NbO_{10}$ (Ln = La, Pr, Nd, Sm) with the new type ordering sequence, although their size and charge differences are not significant. The ordering behavior in the layered perovskites should be viewed with consideration to the electrostatic effect of the interlayer, in addition to the size and charge differences. It is, therefore, necessary to readdress the distribution of B-site cations in layered perovskite compounds such as $Bi_3PbTi_2NbO_{12}$ and $Rb_2Sr_2TiNb_2O_{10}$.

Acknowledgements

Y.-S. Hong gratefully acknowledges the financial support for this work by the Ministry of Education (BK21).

References

1 B. Frit and J. P. Mercurio, *J. Alloys Compd.*, 1992, **188**, 27.
2 P. D. Battle, M. A. Green, N. S. Laskey, J. E. Millburn, L. Murphy, M. J. Rosseinsky, S. P. Sullivan and J. F. Vente, *Chem. Mater.*, 1997, **9**, 552.
3 M. Dion, M. Ganne and M. Tournoux, *Mater. Res. Bull.*, 1981, **16**, 1429.
4 A. J. Jacobson, J. W. Johnson and J. T. Lewandowski, *Inorg. Chem.*, 1985, **24**, 3727.
5 J. Gopalakrishnan, V. Bhat and B. Raveau, *Mater. Res. Bull.*, 1987, **22**, 413.
6 M. A. Subramanian, J. Gopalakrishnan and A. W. Sleight, *Mater. Res. Bull.*, 1988, **23**, 837.
7 R. A. Mohan Ram and A. Clearfield, *J. Solid State Chem.*, 1991, **94**, 45.
8 S. Uma and J. Gopalakrishnan, *J. Solid State Chem.*, 1993, **102**, 332.
9 S. Uma and J. Gopalakrishnan, *Chem. Mater.*, 1994, **7**, 6.
10 Y.-S. Hong and S.-J. Kim, *Bull. Korean Chem. Soc.*, 1996, **17**, 730.
11 Y. Ebina, A. Tanaka, J. N. Kondo and K. Domen, *Chem. Mater.*, 1996, **8**, 2534.
12 T. Takata, Y. Furumi, K. Shinohara, A. Tanaka, M. Hara, J. N. Kondo and K. Domen, *Chem. Mater.*, 1997, **9**, 1063.
13 A. J. Jacobson, J. W. Johnson and J. T. Lewandowski, *Mater. Res. Bull.*, 1987, **22**, 45.
14 J. Gopalakrishnan and V. Bhat, *Inorg. Chem.*, 1987, **26**, 4301.
15 J. Gopalakrishnan, S. Uma and V. Bhat, *Chem. Mater.*, 1993, **5**, 132.
16 Y.-S. Hong and S.-J. Kim, *Bull. Korean Chem. Soc.*, 1997, **18**, 623.
17 S.-H. Byeon, H. Kim, J.-J. Yoon, Y. Dong, H. Yun, Y. Inaguma and M. Itoh, *Chem. Mater.*, 1998, **10**, 2317.
18 J. Rodriguez-Carvajal, Program FULLPROF, version 3.2, January 1997, LLB JRC.
19 K. Toda and M. Sato, *J. Mater. Chem.*, 1996, **6**, 1067.
20 M. P. Crosnier-Lopez, H. Duroy and J. L. Fourquet, *Mater. Res. Bull.*, 1999, **34**, 179.
21 N. S. P. Bhuvanesh, M. P. Crosnier-Lopez, H. Duroy and J. L. Fourquet, *J. Mater. Chem.*, 1999, **9**, 3093.
22 K. Park and S.-H. Byeon, *Bull. Korean Chem. Soc.*, 1996, **17**, 168.
23 N. S. P. Bhuvanesh and J. Gopalakrishnan, *J. Mater. Chem.*, 1997, **7**, 2297.
24 K. Toda, Y. Kameo, M. Fujimoto and M. Sato, *J. Ceram. Soc. Jpn.*, 1996, **102**, 737.
25 N. E. Brese and M. O'Keeffe, *Acta Crystallogr., Sect. B*, 1991, **B47**, 192.
26 A. J. Wright and C. Greaves, *J. Mater. Chem.*, 1996, **6**, 1823.
27 J.-H. Choy and S.-J. Kim, *Mol. Cryst. Liq. Cryst.*, 1998, **311**, 429.
28 K. Toda, M. Takahashi, Z-.G. Ye, M. Sato and Y. Hinatsu, *J. Mater. Chem.*, 1999, **9**, 799.
29 P. M. Woodward, *Acta Crystallogr., Sect. B*, 1997, **B53**, 32.